Physics – Uspekhi **58** (11) 1059 – 1073 (2015)

REVIEWS OF TOPICAL PROBLEMS PACS numbers: **67.80. – s**, **81.10. – h**

Amazing growth of helium crystal facets

V L Tsymbalenko

DOI: 10.3367/UFNe.0185.201511b.1163

Contents

Abstract. This review systematizes experimental data from the study of two unusual phenomena: the superslow growth of a perfect, growth-defect-free crystal facet, and the abrupt transition of a crystal facet to an anomalous state with a growth rate greater by two to three orders of magnitude than the normal value (the 'burstlike growth effect').

Keywords: quantum crystals, kinetics of crystal growth, low temperature physics

1. Introduction

The great variety of forms of crystal growth is fairly well explained in terms of the theory of layer-by-layer growth based on explicit energetic and geometric considerations. For example, the attachment of a single atom to a flat crystal surface is energetically disadvantageous, since it tends to chiefly enlarge the facet area having a positive energy. This accounts for the cooperative 'adhesion' of a compact atomic conglomerate, i.e., a two-dimensional nucleus of the atomic height. In this case, the net energy gain proportional to the object volume (nucleus area) exceeds the positive contribution proportional to the object perimeter (boundary length). Such a picture facilitates a qualitative understanding of the mechanism underlying the growth of a perfect crystal facet, its kinetics being determined by the fluctuational passage over the energy barrier for the formation of the seed of a new layer. Characteristic kinetic patterns are the exponential dependence on the thermodynamic force (the difference $\delta\mu$ in chemical potential between the phases) and the sharp drop in the growth rate with decreasing temperature if the energy barrier is overcome via thermal fluctuations.

Another, more efficient, growth mechanism is related to the imperfection of facets with bending steps. The attachment of an atom to a step kink does not change the facet surface area, i.e., the energy, and is therefore a barrierless process. Then, the facet growth rate is limited by the presence of bending steps. A step running at an angle to the close-packed direction has the necessary kinks as follows from its geometry. Topologically irremovable step sources are formed on the facets by screw dislocation outcrops. A step originating from a single dislocation coils into a spiral in the course of growth. The rate of facet growth by this mechanism is proportional to the square of the thermodynamic force. A pair of screw dislocations emerging on the surface makes up a Frank–Read source that starts functioning when the threshold determined by the step linear energy and the distance between the dislocation outcrops is exceeded. A review of theoretical approaches and collected experimental data as proof of the layer-by-layer growth mechanism for a variety of materials can be found in Ref. [1].

Thus far, we have considered the state of the facets in which surface defects (steps) have a positive linear energy. As the temperature rises to a certain critical value, the free energy of the step may fall to zero. When this critical temperature,

V L Tsymbalenko National Research Centre 'Kurchatov Institute', pl. Akademika Kurchatova 1, 123182 Moscow, Russian Federation
E-mail: VLT49@yandex.ru

Received 22 April 2015, revised 31 August 2015
Uspekhi Fizicheskikh Nauk **185** (11) 1163 – 1178 (2015)
DOI: 10.3367/UFNr.0185.201511b.1163
Translated by Yu V Morozov; edited by A Radzig

i.e., roughening phase transition temperature T_R, is exceeded, barrierless step formation occurs. In accordance with the above considerations, this causes qualitative changes in the growth kinetics of crystal surfaces. For $T < T_R$, a crystal has flat portions (atomically smooth surfaces) that become rounded (atomically rough) as $T > T_R$. Accordingly, the surface growth rate in the former case is determined by two-dimensional nucleus formation and step sources, whereas in the latter case the surface grows evenly at a rate proportional to the applied supersaturation. The roughening transition temperature T_R depends on such surface parameters as energy and interplanar spacing.

Experimental studies of the mechanisms behind facet growth kinetics encounter difficulties, because the growth rate being measured depends on both the kinetics of atomic attachment to the surface and transport fluxes in the bulk controlled by thermal conduction which ensures removal of crystallization heat, and by viscosity influencing mass inflow. With these factors in mind, it is desirable to choose study objects with high heat conductivity and minimal fluid viscosity. Under these conditions, the process of helium crystallization is optimal at temperatures below the superfluid transition point, when the thermal conductivity of liquid helium is extremely high, while viscosity is low and tends to zero as the temperature falls. An additional advantage is that crystallization heat becomes negligibly small with decreasing temperature. The quantum nature of helium crystals is manifested as spreading of the liquid–solid interface and step kink delocalization [2]. The mobility of such kinks governed by scattering from fluid and crystal quasiparticles (phonons and rotons) increases with decreasing temperature; in turn, it is manifested as the observed enhancement of the kinetic coefficient of the atomically rough surface growth. Experimental studies of the growth kinetics of helium crystal facets at minor departures from equilibrium have demonstrated qualitative and quantitative agreement with the layer-by-layer growth model (see Ref. [3] for its main features).

However, the enhanced degree of departure from equilibrium is associated with an unexpectedly sharp change in the growth kinetics of helium crystal facets observed in experiment. The growth rate increases abruptly by two–three orders of magnitude (so-called burstlike growth). Such an effect cannot be explained in terms of the above considerations. Researchers have failed to account for the nature of the enigmatic transition to the fast growth state during the two decades that have passed since the discovery of this phenomenon. Another amazing phenomenon is the superslow growth of crystal facets having no sources, such as screw dislocation outcrops on the surface. This review presents results of experimental studies of the aforementioned phenomena.

2. Experimental techniques

2.1 Specific features of the phase diagram of crystalline helium

Unlike the phase diagram of conventional materials, the phase $(T-p)$ diagram of helium isotopes has no triple point: helium remains in the liquid state at a pressure of saturated helium vapors as temperature drops to absolute zero (see the phase diagram of ^{4}He in Fig. 1). The solid phase forms at a pressure of above 25 atm. The phase curve is practically horizontal in the temperature range of interest. A small minimum at 0.78 K corresponds to a pressure 7.5 mbar lower than the solidification pressure at absolute zero [4]. At temperatures below ≈ 1.45 K, helium crystallizes into a hexagonal close-packed structure with the ratio c/a between unit cell edges close to the value for a solid ball packing.

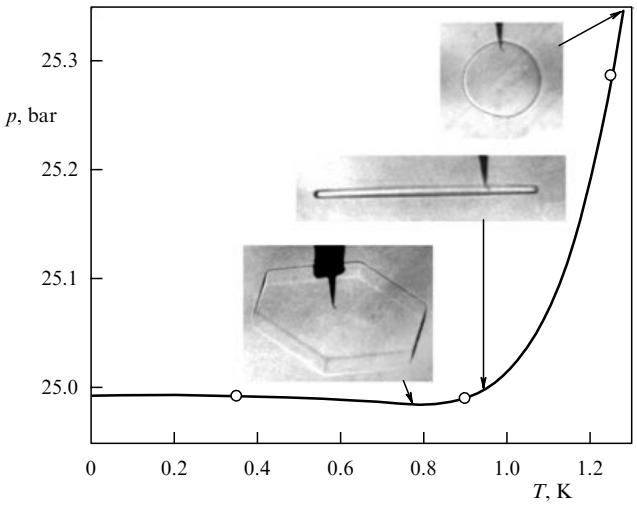

Figure 1. Phase $T-p$ diagram of ^{4}He. White dots denote the roughening temperature of *s*-, *a*-, and *c*-facets (see the text). The insets depict crystal growth forms in the temperature ranges shown.

As temperature decreases, the facets for three crystallographic orientations become visually apparent. The basal plane (0001) is the first to be faceted at $T_{R1} \approx 1.25$ K (*c*-facets). As temperature continues to fall to $T_{R2} \approx 0.9$ K, the $(10\bar{1}0)$ planes become faceted (*a*-facets). For $T < T_{R2}$, the freely growing crystal takes the shape of a hexagonal prism, with atomically rough edges retained. The third roughening transition occurs on planes $(10\bar{1}1)$ at $T_{R3} \approx 0.35$ K (*s*-facets).

Figure 1 shows the growth pattern of a freely growing crystal in three temperature ranges, viz. above the first roughening transition, between the first and second, and between the second and third.

2.2 Measurement of the crystal surface growth rate

Optical methods are used for direct measurements of the crystal surface growth rate. One of them consists in filming the growth process that allows the surface position to be determined with an accuracy of ≈ 0.03 mm. This technique was employed when viewing the shape of crystals in a cryostat with a horizontally arranged optical axis (Fig. 2) [5, 6]. Helium being transparent in the visible range and having a close-to-unity refraction coefficient $n = 1.0252$, only crystal contours and edges are discernible when viewed against the light. If the angles between the facets are known, the whole crystal shape can be unambiguously reconstructed from the two-dimensional projection. This method makes possible simultaneous measurements of the growth rate of all crystal facets.

The interferometric technique [7, 8] has been applied for more accurate measurements of the position and growth rate of the basal *c*-facet (Fig. 3). A vertical laser beam was reflected from the crystal surface and a semitransparent mirror, producing an interference pattern recorded by a refrigerated CCD-camera. Resolution reached in measuring the surface vertical shifts amounted to 3 nm. The growth rate of *a*-facets parallel to the light ray was measured in these experiments from the shift of facet images to a positional accuracy of 0.025 mm [8].

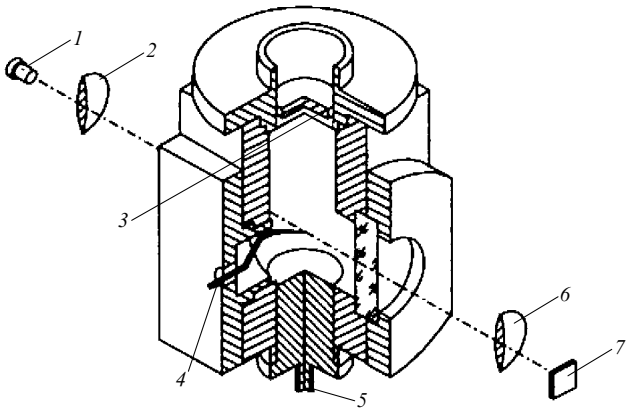

Figure 2. Schematic diagram of an optical container for the free growth of helium crystals. *1* — pulsed infrared light-emitting diode, *2* — collimator, *3* — capacitive sensor membrane, *4* — tungsten needle on which crystal growth was initiated, *5* — copper cold conductor, *6* — objective, *7* — CCD-camera (CCD — charge-coupling device).

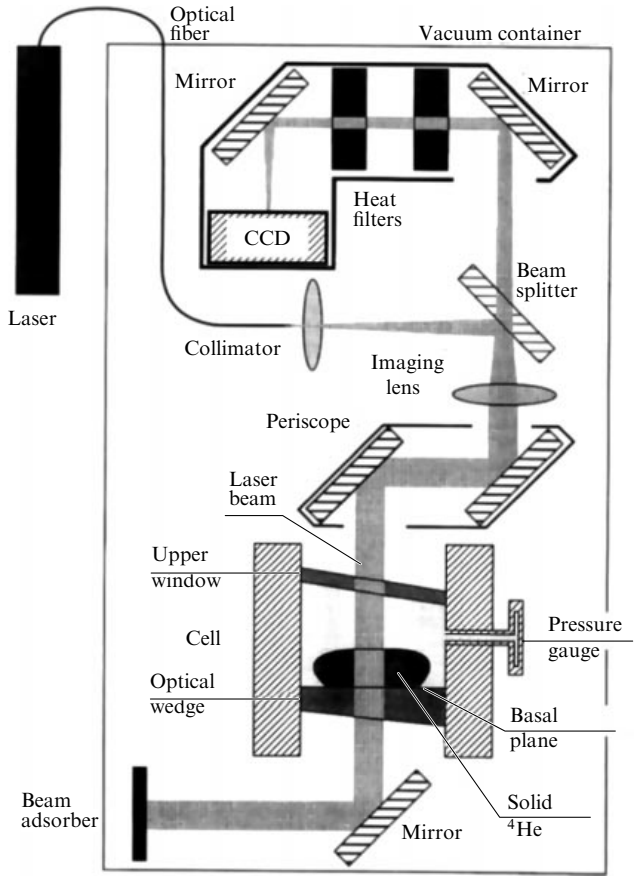

Figure 3. Interferometer and cryogenic part of a dissolution refrigerator for the study of *c*-facet growth kinetics in the millikelvin temperature range.

Variation of pressure inside the container serves as a parameter reflecting the crystal growth rate. The requirement that the heat inflow be small in a capillary connecting the external pressure system to the container with a temperature close to absolute zero accounts for the high hydrodynamic impedance of the capillary and, as a result, for the large times needed to set the pressure to equilibrium with the external pressure system. In the experiments being considered, these times were longer than the time of unusual crystal growth; therefore, it can be supposed with a high accuracy ($\sim 10^{-4}$) that the helium mass in the container remained constant during the process. Pressure $p(t)$ in the container begins to decrease during the growth process, because the densities of the liquid and solid phases are different; it falls to a phase equilibrium value of p_{phase} when growth is complete. The volume of the growing crystalline phase is deduced from the law of conservation of mass:

$$V_{\text{cryst}}(t) = V_0 \frac{\rho_l}{\Delta\rho} k_l \big(p_0 - p(t)\big) . \qquad (1)$$

Here, V_0 is the inner container volume, k_l is the compressibility, p_0 is the starting pressure, p is the density, and $\Delta\rho = \rho_s - \rho_l$. Subscripts s and l refer to the solid and liquid phases, respectively. The crystal volume increases during free growth due to the growth of all facets, and the averaged growth rate reflects growth in all crystallographic directions. Interferometric measurement of the growth of a separate facet gives the growth rate of the basal facet.

2.3 Creation of high degrees of departure from equilibrium

After the quantum kinetics of atomically rough surfaces had been predicted [2] and observed [9], researchers centered attention on these objects. Facet kinetics were investigated incidentally; the results of measurements failed to reveal any peculiarities and were interpreted in the framework of the theory of layer-by-layer growth of crystals.

In the first experiments, supersaturation was created by a hydrostatic pressure gradient, and it was limited by the height of the liquid column in the container. As a result, the supersaturation pressure did not exceed ≈ 100 μbar [10].

Higher supersaturation pressures, up to ≈ 1 mbar, have been obtained in experiments in which the fluid is injected into the container using an external pressure control system [11]. These experiments were motivated by the following consideration. Since the growth rate at low supersaturations is determined by surface defects with a power-law dependence on supersaturation pressure, the growth regime sustained by two-dimensional nucleation with its exponential $\delta\mu$-dependence should prevail at large magnitudes of departure from equilibrium. We sought to reach a temperature region in which two-dimensional nuclei appear at the facets in a quantum mode, as predicted by Andreev [12] (see also paper [13]).

A marked increase in supersaturation pressure (to 3–50 mbar) was achieved by a method in which crystal nucleation originated in a metastable fluid [14] (see Fig. 2). Under these conditions, the maximum degree of supersaturation was limited by spontaneous nucleation of a crystal on the wall of the container. An additional electrostatic pressure generated by the application of a high-voltage pulse ≈ 30 μs in duration to a tungsten needle tip was used to initiate nucleation at intermediate supersaturations. Crystal growth in the millikelvin temperature region (see Fig. 3) was induced by fluid inflow into the container [8]. The resulting supersaturation pressure depended, as in experiment [11], on the balance between the inflow velocity and the facet growth rate and did not exceed 2 mbar.

2.4 Determination of the growth driving force and growth kinetic coefficient in a quasistationary state

The growth of the crystal surface is caused by supersaturation, i.e., the chemical potential difference $\delta\mu$ between the

phases. The supersaturation is created either by overcooling the system or by increasing pressure relative to the phase equilibrium pressure. In the temperature range being considered, supersaturation was achieved with the latter technique, bearing in mind the nearly horizontal $p_{\rm phase}(T)$ curve (see Fig. 1). Because crystal growth takes less time than characteristic heat and mass exchange times, i.e., occurs at almost constant entropy and mass, the chemical potential difference $\delta\mu$ between the phases per mass unit is defined by the expression [14]

$$\begin{aligned}
&\delta\mu = -(S_{\rm l} - S_{\rm s})\Delta T + \left(\frac{1}{\rho_{\rm l}} - \frac{1}{\rho_{\rm s}}\right)\Delta p\,,\\
&\Delta T = \Delta p\,\frac{\beta_{\rm l} - k_{\rm l}\,{\rm d}p/{\rm d}T}{C_p/T - \beta_{\rm l}\,{\rm d}p/{\rm d}T}\,,\\
&\delta\mu = \alpha(T)\,\frac{\Delta\rho}{\rho_{\rm l}\,\rho_{\rm s}}\,\Delta p\,.
\end{aligned} \tag{2}$$

Here, S is the entropy per mass unit, C_p is the heat capacity of the fluid under constant pressure, β is the thermal expansion coefficient, and ${\rm d}p/{\rm d}T$ is the slope of the phase equilibrium curve. Coefficient $\alpha(T)$ at temperatures below 1 K differs from unity by less than 2%, and $\alpha(T) \to 1$ as $T \to 0$; therefore, the degree of departure from phase equilibrium is determined to high accuracy by the excess of pressure over the phase equilibrium pressure.

In both methods, the pressure inside the container was measured by a capacitive sensor. In experiments conducted in the container shown in Fig. 2, the membrane was part of its wall with a vibration eigenfrequency of ≈ 28 kHz, which allowed pressure to be measured with a time step of 50 μs. In the method illustrated by Fig. 3, the sensor was placed near the container and connected to it by a capillary, which enlarged the time step of pressure measurements to ≈ 0.5 s.

2.5 Method for the measurement of the growth kinetics of helium crystal facets in the oscillatory mode

Simultaneous measurement of the facet growth rate and pressure gives the sought dependence $V(\delta\mu)$ with an important proviso that both methods measure pressure at a distance from the growing crystal rather than supersaturation pressure on the surface. This circumstance is unessential at low growth rates and correspondingly pressure gradients, but sensor readings begin to differ significantly from the values at the crystal–fluid interface as the crystal growth rate increases. Pressure variations in this mode of operation are illustrated by Fig. 12 in Section 4. The pressure at the wall does not coincide with that on the crystal surface, is of a vibrational character, and can be lower than the phase equilibrium pressure. Its vibrations reflect excitation of natural acoustic vibrations of the fluid inside the container, whose frequency and damping depend on experimental geometry, i.e., the internal configuration of the container, the shape of a crystal, and the kinetics of its surface.

A simplified model was constructed for the quantitative estimation of the crystal growth rate. It was assumed that both the crystal and the inner surface of the container are spherical in shape, while the kinetic coefficient of growth is isotropic. This scenario left beyond consideration such issues as the nonuniformity of the acoustic field at the boundary of a crystal, which is responsible for the different growth rates of its facets, the anisotropy of the growth kinetic coefficient, and its possible nonlinear dependence on the applied supersaturation pressure, which differs for different facets. Only the growth kinetic coefficient averaged over the crystal surface for the time of the first vibration half-period can be determined.

The equation for the growth of a crystal with radius r_0 in a container of radius R ($r_0 \ll R$) in an ideal fluid has the form [15]

$$\Delta\phi - \frac{1}{c_{\rm l}^2}\,\frac{\partial^2\phi}{\partial t^2} = 0\,, \qquad \mathbf{v} = \nabla\phi\,, \qquad p = -\rho_{\rm l}\,\frac{\partial\phi}{\partial t}\,, \tag{3}$$

where $c_{\rm l}$ is the speed of sound, with the boundary conditions

$$v_r(R) = 0\,, \qquad v_r(r_0) = -K\left(\frac{\Delta\rho}{\rho_{\rm l}}\right)^2\frac{1}{\rho_{\rm s}}\,p\,, \tag{4}$$

$$V = K\,\frac{\Delta\rho}{\rho_{\rm l}\,\rho_{\rm s}}\,p\,. \tag{5}$$

Here, V is the boundary growth rate, p is the pressure counted from the phase equilibrium pressure, and K is the growth kinetic coefficient. The limiting case $K = 0$ gives liquid vibration modes in a rigid container with a minimum frequency $\omega_0 \approx 4.5c/R \sim 25$ kHz at $R \sim 1$ cm. In the fast kinetics case of $cK \gg 1$, a soft mode appears, having the crystal size-dependent frequency

$$\omega_{\rm soft} = \frac{c}{R - r_0}\,\sqrt{\frac{3r_0}{R - r_0}} \approx \frac{c\sqrt{3}}{R^{3/2}}\,r_0^{1/2} \approx 0.39\omega_0\,\sqrt{\frac{r_0}{R}} \tag{6}$$

falling in a range of roughly 2–5 kHz at initial supersaturation pressures of 1–20 mbar.

The kinetic coefficient of facet growth in an anomalous state was obtained through numerical treatment of the first vibration half-period by solving the set of equations (3), (4) and taking into account that the size of the crystal changes from zero to maximum [16]. Within this time range, it is the slowest-growing portions of the crystal surface, i.e., the facets, that determine the overall growth rate. After the averaged growth kinetic coefficient K is calculated from anisotropy measurements in video images, the kinetic coefficients of a- and c-facet growth are found. Further vibrations involve atomically rough parts of the surface, the contribution from which is difficult to estimate. Therefore, these fragments of video recordings were disregarded.

3. Normal growth of helium crystal facets

The main features of the normal growth of helium crystal facets are as follows: the facet growth depends on the crystal's previous history, e.g., mechanical impacts it experienced; equivalent a-facets grow at different rates; the growth rate shows nonlinear dependence on supersaturation pressure; there is a threshold, i.e., supersaturation, above which the facet growth begins. The available experimental data are collected in Fig. 4 [8, 10, 11, 17] illustrating the temperature dependence of the 'growth kinetic coefficient K' for a- and c-facets. The dashed line plots this dependence for an atomically rough surface [19, 20]. The growth kinetic coefficients presented in the figure were obtained by approximating nonlinear $V(p)$ dependences with a linear function in accordance with definition (5). It provided a rough order-of-magnitude estimate of facet mobility. Although the data obtained at different supersaturations are subject to a considerable scatter, they reveal the general dependence of

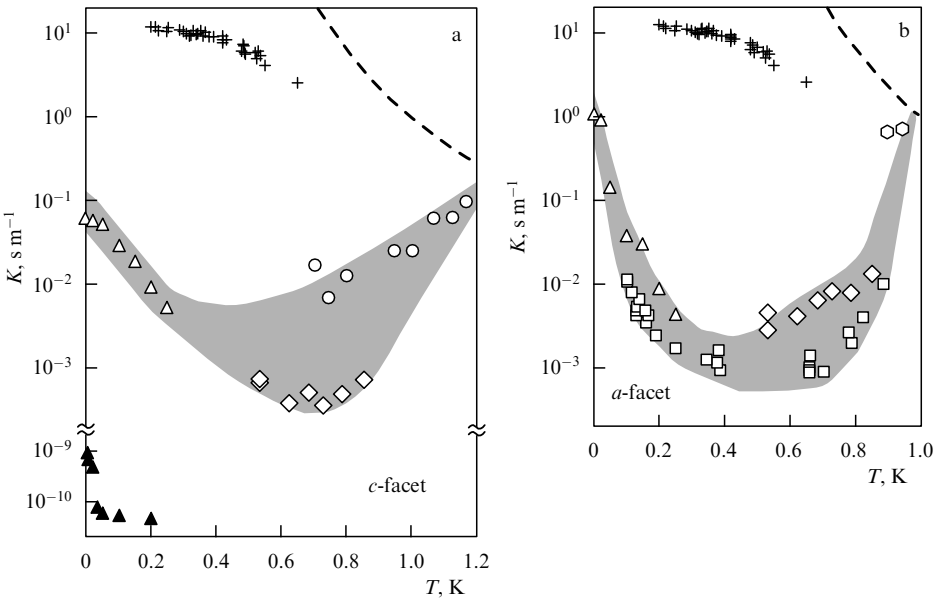

Figure 4. Temperature dependences of *c*-facet (a) and *a*-facet (b) growth coefficients. Light symbols refer to the crystals whose facet kinetics are controlled by growth sources: triangles — [8], squares — [10], diamonds — [11], circles and hexagons — [17]. Black triangles: superslow growth of the perfect facet [7, 8]. Crosses: facet kinetics in the burstlike growth regime [18].

facet kinetics on temperature. At temperatures close to the roughening transition temperature, the growth rates of the facets and atomically rough surfaces are very similar. As temperature drops, the facet mobility decreases, but the growth kinetic coefficient increases at temperatures beginning from about 0.4–0.6 K, suggesting a rise in the facet growth rate. S Balibar and co-workers proposed an explanation for this dependence, based on a spiral growth model [10]. The rate v_d of the spiral growth is directly proportional to step mobility k_{step} and inversely proportional to the step linear energy β: $v_d \sim K \sim k_{step}/\beta$. The step mobility increases monotonically with a drop in temperature, whereas the β energy increases to a constant value. The authors of Ref. [10] attributed nonmonotonic behavior of facet mobility to the competition between these two processes.

To sum up, the growth kinetics of helium crystal facets at low supersaturations are fairly well explained in terms of the known layer-by-layer growth mechanisms by virtue of spiral growth and Frank–Read sources. A description of growth at temperatures below 100 mK requires taking account of step inertia and 'relativistic' effects related to step acceleration up to the speed of sound, even at modest supersaturations, as shown by Hakonen et al. [7].

4. Anomalous growth of helium crystals

4.1 First observations of crystal transition to an anomalous state

The phenomenon of anomalously rapid growth of helium crystals was discovered from a pressure jump simultaneously and independently by a Russian team and a Russian–Finnish team in 1996 [21, 22]. Interference measurements were performed in an optical dissolution cryostat. As a fluid was constantly injected into the container, the pressure increased monotonically till it dropped abruptly, jumpwise, which suggested rapid growth of the *c*-facet (Fig. 5a).Then, the facet returned to the initial state and the process was repeated. The short time of the pressure drop gave evidence of a

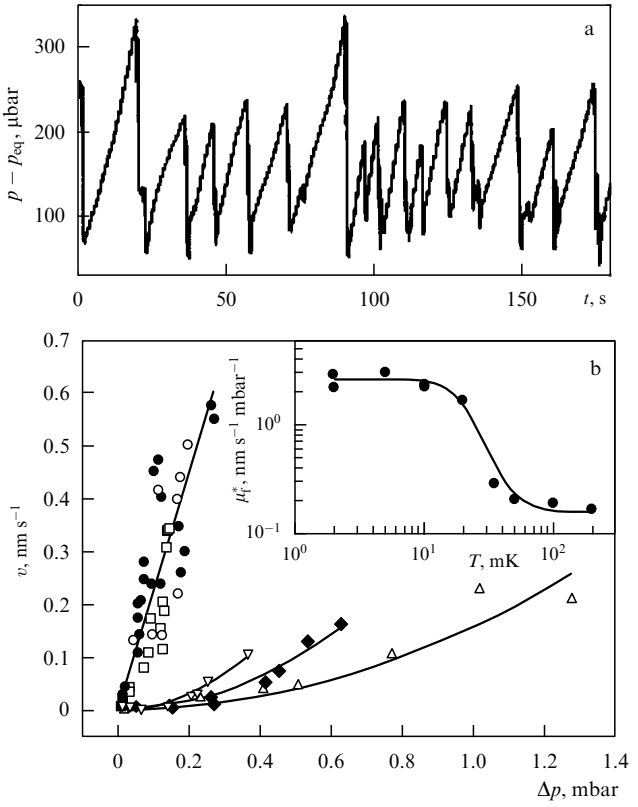

Figure 5. (a) Sawtooth pressure pattern under conditions of constant fluid injection into a container containing a crystal with a perfect *c*-facet at the bottom [7]. (b) Growth rates of this facet at 2 mK (white circles), 10 mK (squares), 20 mK (black circles), 50 mK (upside down triangles), 100 mK (diamonds), and 200 mK (right-side up triangles). Inset plots temperature dependence of *c*-facet mobility.

qualitative change in the kinetics, i.e., the anomalously fast growth of the perfect facet [21].

In experiments on solid phase nucleation in a metastable fluid carried out in the absence of visual control [22, 23]

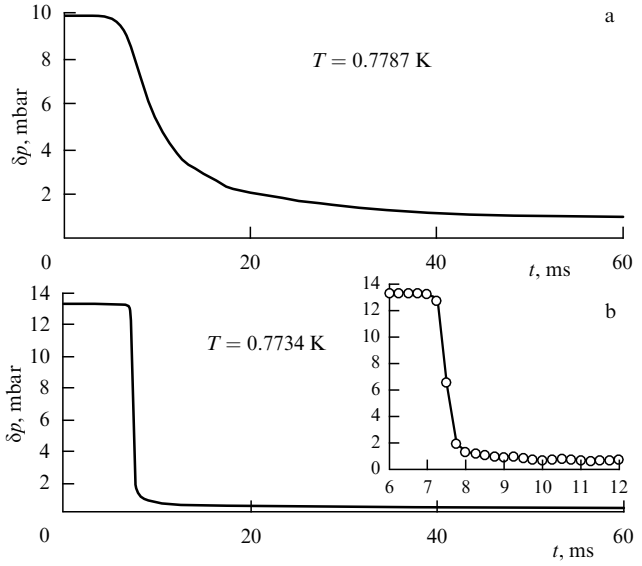

Figure 6. Sharp change in the crystal growth rate upon a 5.3-mK decrease in temperature apparent at the pressure vs time graph [23]. (a) Pressure drop in the container associated with normal crystal growth. (b) Pressure jump in the burstlike crystal growth regime. Inset shows the pressure jump recording with a higher temporal resolution.

(Fig. 6), a pressure jump could not be interpreted unambiguously. It was at first impossible to *a priori* exclude multiple nucleation, which markedly increased the overall surface area of the nuclei; when its slow kinetics were preserved, the overall crystallization rate increased too, while pressure sharply decreased.

Further experiments in an optical ^{3}He cryostat showed that the pressure jump was caused by a sharp change in the facet growth kinetics in a single crystal. Variation of the initial supersaturation by applying an additional electrostatic pressure to the needle tip where the crystal was originated made it possible to construct the first diagram in the supersaturation region in which the crystal performed transition to a burstlike growth mode [24].

The author of Ref. [24] also conjectured a similar character of helium crystal metamorphosis in terms of the temperature dependence of the borderline between the normal and anomalous growth revealed by the two methods and an occurrence of delay between the effect of supersaturation and the transition to the fast growth state.

Results of the first experiments made it clear that the phenomenon sequentially passes through three stages, viz. (1) the formation of a new crystal state under the effect of supersaturation, (2) a jumplike acceleration of the kinetics resulting in the fast growth of the crystal with a drop in pressure to the phase equilibrium pressure, and (3) the return of the facet kinetics to the normal (slow) ones. These stages have been investigated in more detail.

4.2 Crystal prior to the transition to an anomalous state

4.2.1 The slow growth of a perfect crystal. In experiments on the growth of dislocation-free *c*-facets, the supersaturation was set at a constant level, and a change in the surface position was determined from a shift of the interference pattern. It turned out that the facets grew in the absence of growth sources, even if very slowly [21].

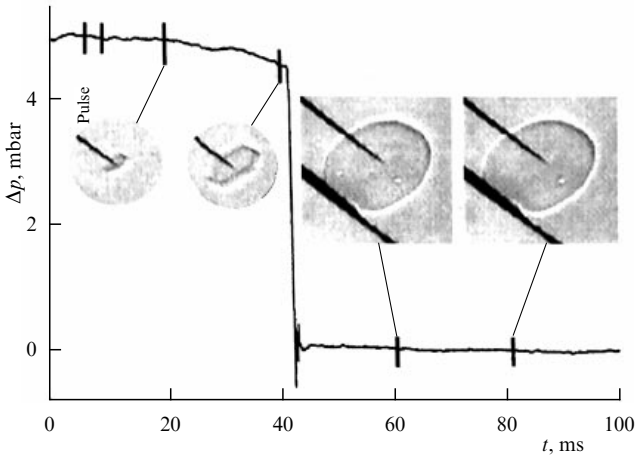

Figure 7. Crystal growth at $T = 0.639$ K (two first stages of the process). Normal growth occurs with a minor anisotropy from pulse-induced crystal formation till pressure jump. The latter is apparent within roughly 38 ms due to a sharp increase in the facet growth rate [16].

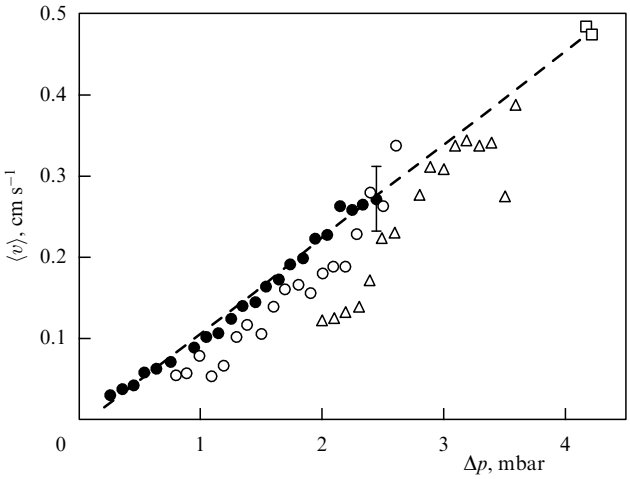

Figure 8. Mean normal crystal growth rates at $T = 0.639$ K (white symbols) obtained prior to the pressure jump deduced from the recordings in Fig. 9. The dependence of the crystal growth rate in the absence of transition to the anomalous state (black circles) [16].

Figure 5b plots growth rates of a *c*-facet in a temperature range of 2–250 mK. The inset demonstrates the temperature dependence of surface mobility $\mu_f^* = v/\Delta p$. The same data recounted from relation (5) are presented in Fig. 4, showing that the growth rate of the perfect facet is 7–8 orders of magnitude lower than that of the facets having growth sources.

4.2.2 Growth kinetics of a defective crystal. A crystal formed at the needle in a metastable fluid possesses defects responsible for the facet growth via irremovable step sources (spiral growth and Frank–Read sources) (Fig. 7). The crystal is shaped like a hexagonal prism, and its equivalent *a*-facets grow at different rates (see Fig. 7), as is typical of facet growth governed by growth defects [11]. Mean facet growth rates calculated from relation (5) for crystals undergoing and not undergoing transition to the fast growth state are displayed in Fig. 8. Variations in pressure recordings accompanying the growth of these crystals are illustrated by Fig. 9. Neither the

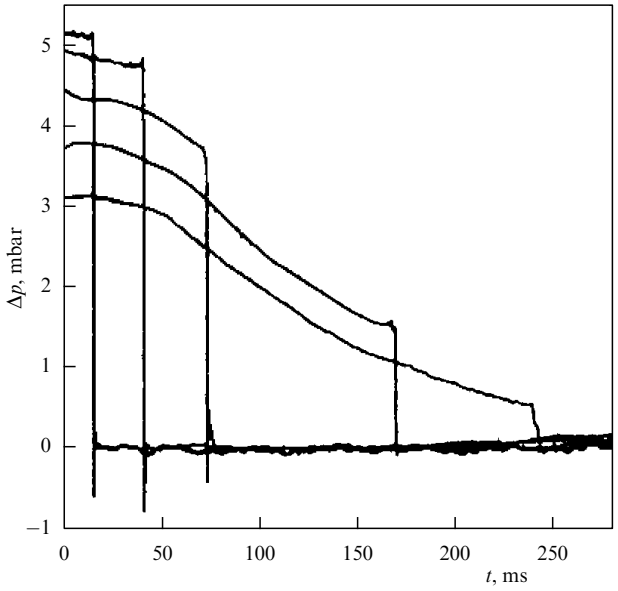

Figure 9. Recordings of pressure drop Δp in the container during crystal growth at $T = 0.639$ K and different initial supersaturations [16].

facet growth rate nor anisotropy before transitions to burstlike growth is significantly different from the respective parameters of normal crystal growth. Against the background of the facet growth rate varying between 0.01 and 0.5 cm s^{-1}, the process described in Section 4.2.1 cannot be observed, even if it takes place. The threshold supersaturation above which the Frank–Read sources begin functioning can be used to estimate dislocation concentration: $\sim 10^5$–10^6 cm^{-2} [11].

4.3 Formation of the anomalous state

Figures 5 and 9 illustrate the first qualitative characteristic of the phenomenon, namely, supersaturation affects a crystal for a long time before the facets pass to the fast growth state. Another qualitative feature is the probabilistic character of the origination of the burstlike growth state. Figure 10a shows cumulative distributions of the supersaturation probability, above which the fast growth of the *c*-facet begins [8], and Fig. 10b plots time lags between crystal nucleation and the pressure jump [17]. Both measurement methods yield similar information on the probability of forming the anomalous state, $W(\Delta p)$ per unit time; specifically, a rise in W shifts the cumulative distribution toward lower supersaturations and decreases the time lag between crystal nucleation and pressure jump. The plots demonstrate two qualitative characteristics of the process: (a) an exponentially fast rise in W with increasing supersaturation, and (b) the influence of temperature (at elevated temperatures, the median is shifted toward high supersaturations, while the time lag increases). In other words, the probability W of burstlike growth origination at constant supersaturation decreases with increasing temperature.

Solid curves in $T-\Delta p$ coordinates in Fig. 11 illustrate the boundaries separating the regions of normal and anomalous crystal growth in pure helium. The boundary for experiments at temperatures of up to 250 mK [8] coincides with the median of distribution shown in Fig. 10a. The curve for temperatures above 0.4 K separates the region in which the kinetics grow jumpwise during the free growth of the crystal at the needle

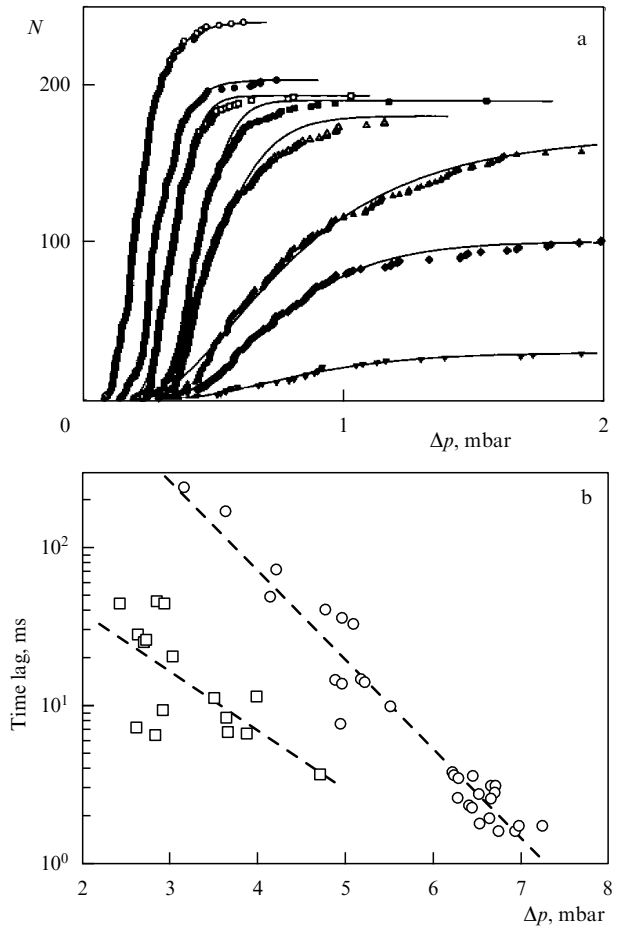

Figure 10. (a) Cumulative distribution of supersaturation at which a jump commences (see Fig. 5); the curves (from left to right) correspond to temperatures of 2, 50, 100, 150, 180, 200, 210, and 250 mK. The distributions are approximated by $\exp(-\text{const}/\delta\mu^2)$ dependence describing quantum formation of two-dimensional nuclei [8]. (b) Plot of pressure drop Δp dependence of time between crystal nucleation on the needle and the onset of its fast growth (see Fig. 9) [16] at $T = 0.639$ K (circles) and $T = 0.48$ K (squares).

from the region in which this process does not occur. It should be noted that such boundaries are conditional due to the probabilistic character of the process and different time periods of supersaturation effects. In experiments with a dislocation-free facet, these times were equivalent to a few dozen seconds (see Fig. 5). For freely growing crystals, the action time of supersaturation was limited by the duration of crystal growth (less than 1 s) (see Fig. 9). This factor weakly affected the phase diagram shown in Fig. 11, because a change in the duration of the supersaturation effect caused only a slight shift of the boundary due to the exponential dependence of W on Δp (see Fig. 10). Taking account of this observation, the boundary supersaturations in both experimental series may be regarded as being in fairy good agreement.

Experimental data presented in Fig. 11 reveal a discrepancy between the results obtained in the millikelvin temperature region [21] and on freely growing helium crystals [17, 25]. In the first series of experiments, it proved impossible for some unknown reasons to preserve the facet free from growth defects after heating above 250 mK. In the second series, the minimal temperature was limited by the characteristics of the ^{3}He cryostat. The addition of the stage of adiabatic

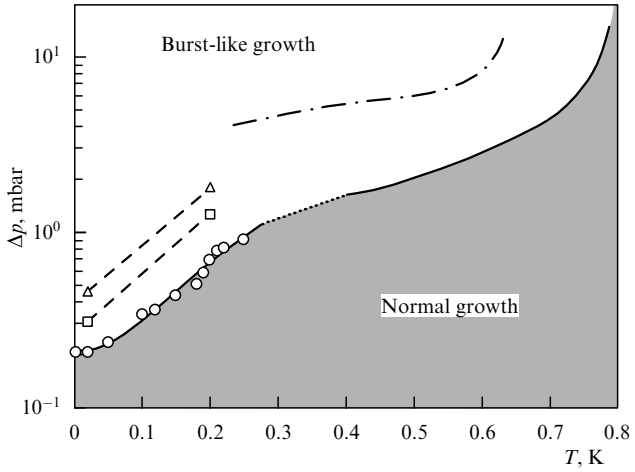

Figure 11. Phase diagram of the region where the burstlike growth state forms. Solid lines denote crystals grown from helium containing less than 0.1 ppm of ^{3}He. Dashed lines separate regions of normal and anomalous crystal growth in a solution containing 10 ppm (squares) and 50 ppm (triangles) of impurity [8]. Dashed–dotted line shows the shift of the boundary separating regions of normal and anomalous crystal growth toward high supersaturations in a solution containing 180 ppm of ^{3}He [33].

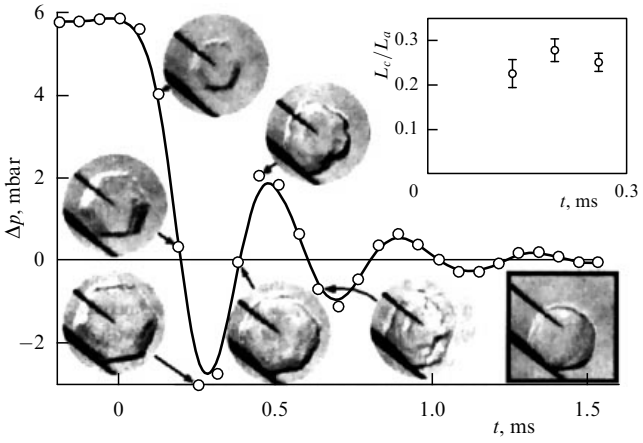

Figure 12. Oscillating growth of a crystal at 0.484 K and an initial supersaturation pressure of 5.8 mbar. In the first crystal vibration half-period, the crystal grows from zero to the maximum size and has kinetic faceting in the form of a hexagonal prism. The growth rate is limited by the facet kinetics. Anisotropy of *a*- and *c*-facets is small. Frame in the bottom right corner shows the crystal shape after completion of growth (13.6 ms) [27]. Inset presents changes in the ratio of *a*- to *c*-facet projections for the first three images.

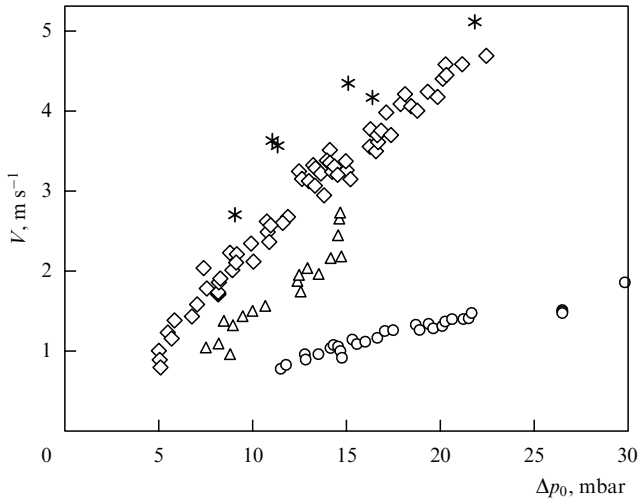

Figure 13. Mean growth rate of crystals created on the needle in the burstlike mode depending on initial supersaturation at 0.653 K (circles), 0.533 K (squares), 0.421 K (diamonds), and 0.206 K (asterisks) [18].

demagnetization of the paramagnetic salt made it possible to decrease the temperature to 180 mK and combine the two parts of the phase diagram [26]. It turned out that the line separating the regions of normal and anomalous growth determined on freely growing crystals with a considerable concentration of growth defects is consistent with the data obtained for defect-free facets.

Another important result pertains to the influence of the roughening transition on burstlike growth process. Temperatures in both experimental series [17, 21] fell in the range between roughening transition temperatures, and the problem of the influence of the roughening transition on the burstlike growth effect, specifically the influence of near-T_R temperature, remained unresolved. Measurements in a temperature range of 0.18–0.4 K, i.e., above or below the temperature of *s*-facet transition to the atomically smooth state, $T_{R3} \approx 0.35$ K, failed to reveal the influence of the roughening transition either on the phase diagram or crystal growth kinetics in the anomalous state. This means that the *s*-facet kinetics are accelerated simultaneously with and in proportion to those of *a*- and *c*-facets (see Fig. 4 and Fig. 13 in Section 4.4).

4.4 Facet growth kinetics after transition to an anomalous state

In experiments on the burstlike growth of *c*-facets [21], the inertia of the pressure gauge (≈ 0.5 s) and long recording times of interference patterns did not allow the fast growth rate to be determined. In experiments on the free growth of crystals in the center of a container, the pressure measurement time constant was ≈ 50 μs, which made it possible to observe pressure changes in the course of growth (Fig. 12). Also, the method described in Section 2.5 was applied to determine the mean growth kinetic coefficient [16, 27]. Simultaneous filming showed that at this stage, too, the crystal has the shape of a hexagonal prism, while the ratio of *c*- to *a*-facet growth rates is $1:(2-3)$.

The small growth anisotropy (see the inset to Fig. 12) evidences two important facts: first, the growth rates of facets with different orientations increase approximately proportionally; second, time lags between crystal nucleation and the transition to the fast growth state differ but insignificantly for different crystal facets and are much smaller than the length of the first pressure oscillation half-period of ≈ 200 μs, i.e., the time of crystal growth with vanishing supersaturation. An estimation of this difference from the crystal shape anisotropy gives the upper bound of < 40 μs. This is the accuracy with which the facet growth rates are simultaneously accelerated.

Dependences of the mean crystal facet growth rate on the initial supersaturation are depicted in Fig. 13 [18]. The growth rates tend toward zero near the boundary of the anomalous state region. Figure 4 presents the values and temperature dependences of the average growth kinetic coefficient derived from such dependences using relation (5). Clearly, the facet growth rates increase by two–three orders of magnitude, depending on temperature after transition to the burstlike growth mode.

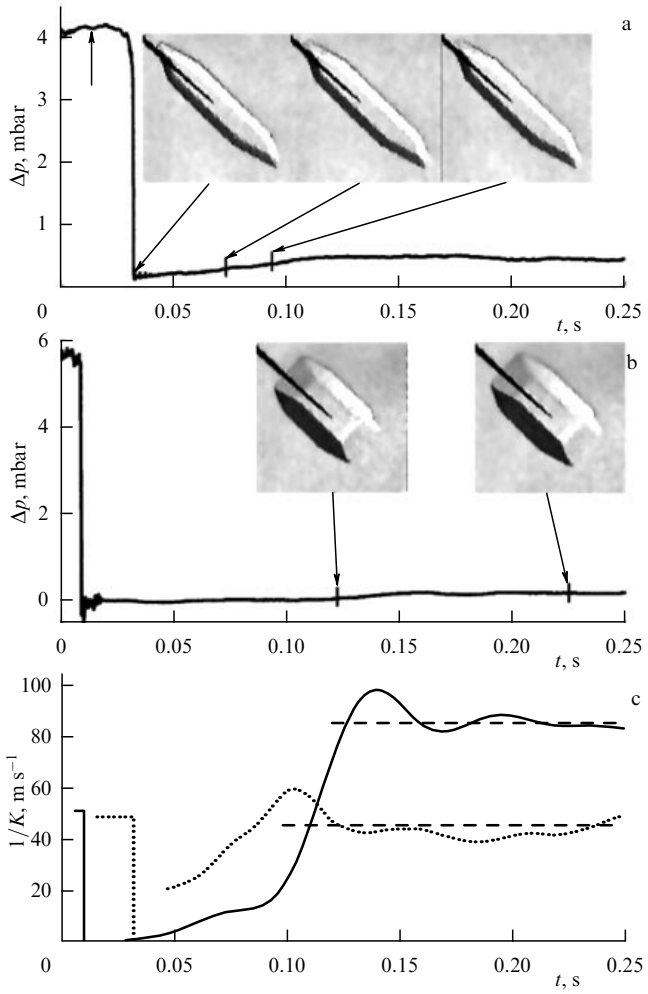

Figure 14. Restoration of slow facet growth kinetics after completion of the fast growth stage (a), $T = 0.69$ K. At high initial supersaturation (b), the time of normal crystal growth till pressure jump is short, and the return to the normal (slow) growth kinetics is delayed. After relaxation, the mean growth kinetic coefficient (c) differs from that measured within the time range from crystal nucleation to the onset of fast growth by less than two-fold [18].

4.5 Return to normal growth kinetics

The closing stage of the process of interest, i.e., the return to normal (slow) facet growth kinetics, was studied using crystals freely grown on a needle [18]. Before growth in a metastable fluid, the pressure inside the container and in the external system was the same and greater than the phase equilibrium pressure. The pressure inside the container fell to below the phase equilibrium pressure after the stage of fast crystal growth was complete, which led to its slow enhancement due to helium inflow from the external system with a time constant of several seconds. At this stage, the pressure in the container depended on the inflow rate and facet growth kinetics. If the parameters of the system are known, it is possible to determine the growth kinetic coefficient K by directly measuring the change in the crystal size [18].

Figure 14 shows pressure recordings during this process and calculated changes of mean facet mobility in crystals grown at different starting supersaturations.

It is worthwhile to mention some essential features of the return to normal growth kinetics. First, restoration of the slow kinetics is a continuous rather than jumplike process taking a few tenths of a second. Moreover, crystals grown far from the boundary separating the normal and anomalous growth regions take more time to restore their normal growth rate. The facet growth kinetics before the pressure jump and after relaxation are very similar. The region between crystal growth termination and the onset of an appreciable pressure rise, in which the kinetics slow down dramatically, remains unexplored because measurements [18] provide information about the closing stage of relaxation of the kinetic coefficient, during which it changes by roughly an order of magnitude.

4.6 Influence of isotopic impurities on the burstlike growth effect

The slowdown of the transition to the anomalous state (Fig. 10b) or the enhancement of boundary supersaturation in the phase diagram in Fig. 11 with an increase in temperature suggested that the latter is related to increased dissipation in the fluid. This parameter can be modified only by introducing an ^{3}He isotopic impurity into superfluid helium to increase the concentration of the normal component. In the experiments reported in paper [8], the density of the normal superfluid helium component at studied impurity concentrations of 10, 50, and 180 ppm matched with impurity concentration at ≈ 0.12, 0.18, and 0.25 K, respectively. In the experiments mentioned earlier, the impurity was removed from helium using the thermomechanical effect, so that the residual ^{3}He concentration was less than 0.1 ppm.

The addition of the impurity not only increased volume dissipation of the fluid but also complicated the picture of crystal growth. The solution phase diagram shows that at low impurity concentrations some of the ^{3}He atoms penetrate into the crystalline phase [28]. The equilibrium concentration of the impurity in the liquid phase is lower at temperatures above ≈ 0.6 K, while in the solid phase for $T \lesssim 0.6$ K. In this region, the impurity barely penetrates into the crystal and is depleted on the surface, which results in enhanced dissipation of the process due to diffusive fluxes [29].

Another phenomenon is associated with the presence of a potential well of depth $E_{ad} \sim 4$ K for impurities at the liquid–solid interface [30–32]. It is responsible for the formation of an adsorption layer decreasing, for example, the surface energy at the interface. This layer is filled up at $T_{ad} \sim E_{ad}/\ln(1/x)$, where x is the impurity concentration in the bulk. For the experimental concentrations of 10, 50, and 180 ppm, one obtains $T_{ad} \approx 0.35$, 0.40, and 0.46 K, respectively.

The introduction of the impurity with a concentration of 10 and 50 ppm in a temperature range of 2–250 mK produced two effects, viz. the superslow growth rate of the dislocation-free c-facet decreased (Fig. 15a), and supersaturations at which it started to grow faster increased (see Fig. 11) [8]. A similar behavior was observed when the crystal grew freely in a temperature range of 0.18–0.75 K [33]. The boundary supersaturation also increased just as the time lags grew between crystal formation instant in the metastable fluid and the pressure jump; in other words, the times of formation of the anomalous state increased (Fig. 15b). Thus, enhanced dissipation in the fluid slowed down both the formation of the anomalous state and the kinetics of superslow crystal growth.

The inference about facet growth rate after transition to the burst-like growth state in Ref. [33] remained a matter of dispute, since the presence of an impurity adds to the difference in chemical potentials of the phases a new factor (impurity concentration at the crystal–liquid interface unmeasurable directly in experiment) that prevents determi-

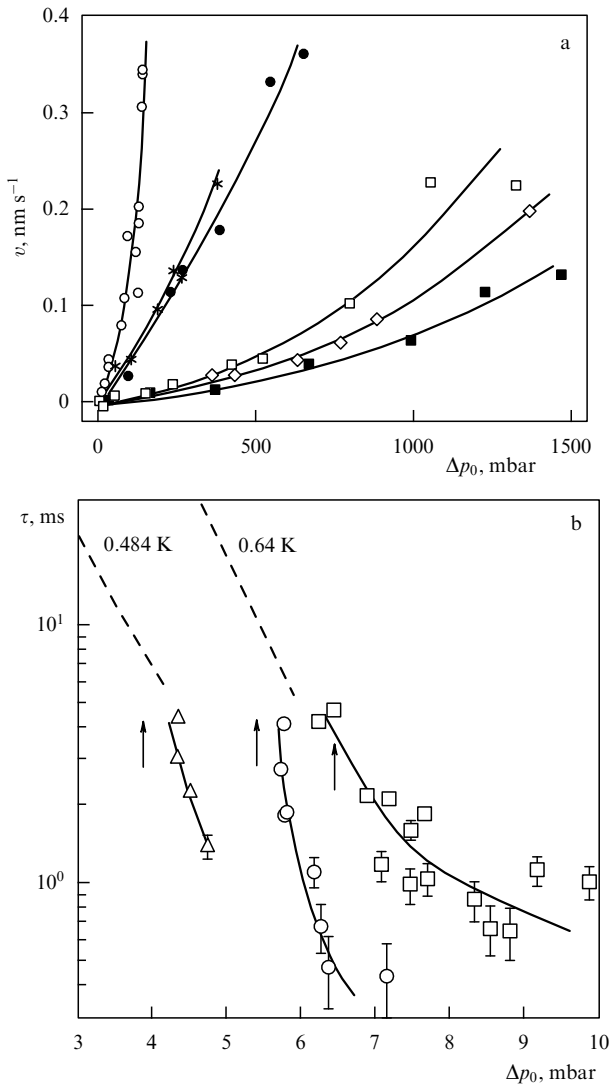

Figure 15. The influence of an ^{3}He impurity. (a) Superslow growth rate of a *c*-facet at two temperatures and three concentrations of the impurity [8]. $T = 20$ mK: white circles — 0.1 ppm, asterisks — 10 ppm, black circles — 50 ppm; $T = 200$ mK: white squares — 0.1 ppm, diamonds — 10 ppm, black squares — 50 ppm. (b) Time of formation of an anomalous state for a crystal freely grown on a needle at an impurity concentration of 180 ppm and 0.24 K (triangles), 0.42 K (circles), and 0.545 K (squares) [33]. Dashed curves show dependences measured in pure helium (Fig. 10b).

nation of the thermodynamic force inducing the crystal growth. The form of pressure drop recordings is becoming more complicated, and they cannot be processed by the method described in Section 2.4.

No peculiarities associated with the point of equal impurity concentrations in the solid and liquid phases at temperatures around 0.6 K or with the formation of the adsorption layer were not observed.

4.7 Bulk properties of the transition

All the above experiments were concerned with changes in the crystal surface kinetics. Two series of experiments were carried out to clarify whether an acceleration of surface growth changes the bulk properties of crystals. The first series was designed to observe transition heat to the anomalous state. Because the near-surface atoms make up only a small part of the total number of atoms in the crystal, only a bulk phase transition was likely to produce an appreciable caloric effect.

The other series was undertaken to indirectly observe changes in the crystal volume properties. It has been known since the 1970s [34–36] that internal friction in the kHz frequency range in crystalline helium is abnormally high, so that the damping decrement reaches ≈ 0.5. The proposed explanation for the nonclassical moment of inertia in solid helium [37, 38] based on the anomaly of internal friction stimulated investigations of this effect [40–44]. At present, the abnormally high dissipation during helium crystal vibrations is interpreted in terms of the Granato–Lucke theory of dislocation damping for movable pinning points [45]. It can be supposed that alteration of bulk properties associated with the formation of the burstlike growth state has an effect on the parameters influencing the oscillation of dislocations, e.g., phonon viscosity, and can manifest itself in the magnitude of internal friction.

4.7.1 Thermal effects accompanying fast crystal growth. The temperature inside the container was measured during crystal growth by a low-inertia superconducting bolometer [46, 47]. The temperature response of the system depends on transition heat, if any, during anomalous state formation, temperature variations associated with adiabatic oscillations of pressure during crystal growth according to relation (2), and a temperature rise due to dissipative growth processes characterized by the growth kinetic coefficient K.

Bolometer temperature recordings are exemplified by Fig. 16. Due to the absence of a noticeable anomaly related to transition heat, only its possible upper bound can be ascertained (less than 1–20% of the system's excess energy before the onset of transition to an anomalous state).

4.7.2 Internal friction in crystals underwent transition to an anomalous state. Internal friction in a crystal after completion of its fast growth stage was measured with the aid of a composite vibrator. The crystal nucleus formed under the effect of a high voltage pulse applied to a tungsten needle tip placed in the gap between the base and the quartz crystal performing free torsional vibrations at a frequency of ≈ 78 kHz (Fig. 17) [48, 49]. Once the growth was completed, the frequency and damping of cooperative vibrations were measured and the contribution of the helium crystal proper was calculated.

These are comparative experiments because measurements at a single frequency do not give unambiguous values for dislocation parameters, such as dislocation concentration and phonon friction of dislocation segments during their vibrations. The time evolution and numerical characteristics of damping (elastic modulus and decrement) of the crystals grown above and below the phase diagram boundary were compared (see Fig. 11). Crystals grown by the conventional method had roughly constant (within $\approx 30\%$) values of both modulus and decrement [49], consistent with those of samples grown over a long period and annealed near the melting curve [36]. Crystals grown in a jumplike mode experienced decrement relaxation from maximum immediately after growth completion to a stationary value (roughly 20 ms) (see Fig. 17). Decrement relaxation recordings normalized to this value were fairly well approximated by the exponential dependence:

$$\frac{\delta(t)}{\delta(20)} = A \exp\left(-\frac{t}{\tau}\right). \qquad (7)$$

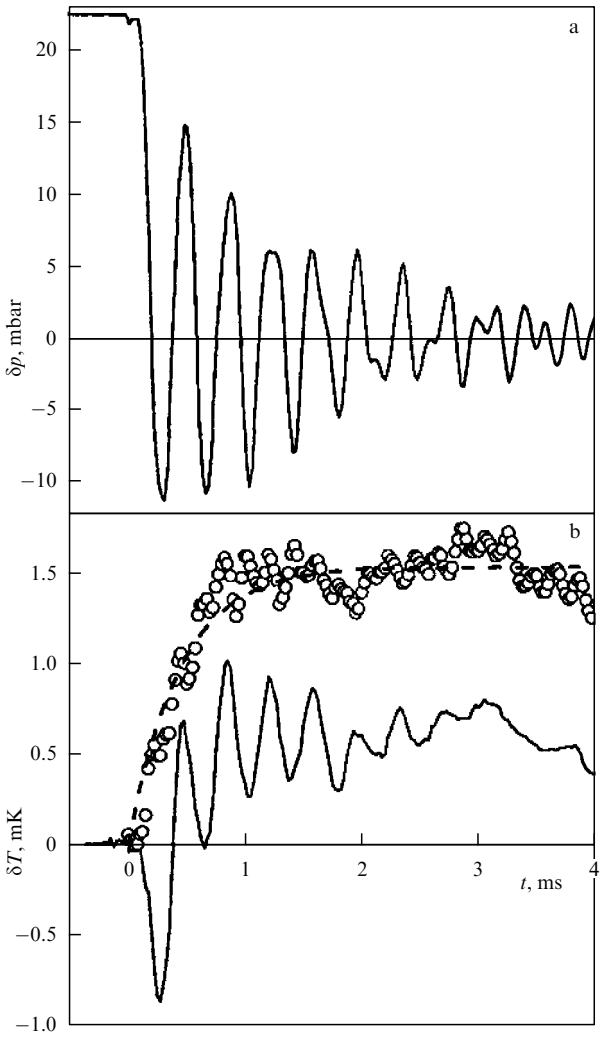

Figure 16. Temperature variations in the container during burstlike growth at $T = 0.40$ K [46]. (a) Pressure oscillation recordings. (b) Temperature fluctuations; circles — results of subtraction from temperature recordings of the oscillating component attributable to adiabatic pressure changes according to formula (2), i.e., the dissipative part of the temperature increment due to growth kinetic coefficient K.

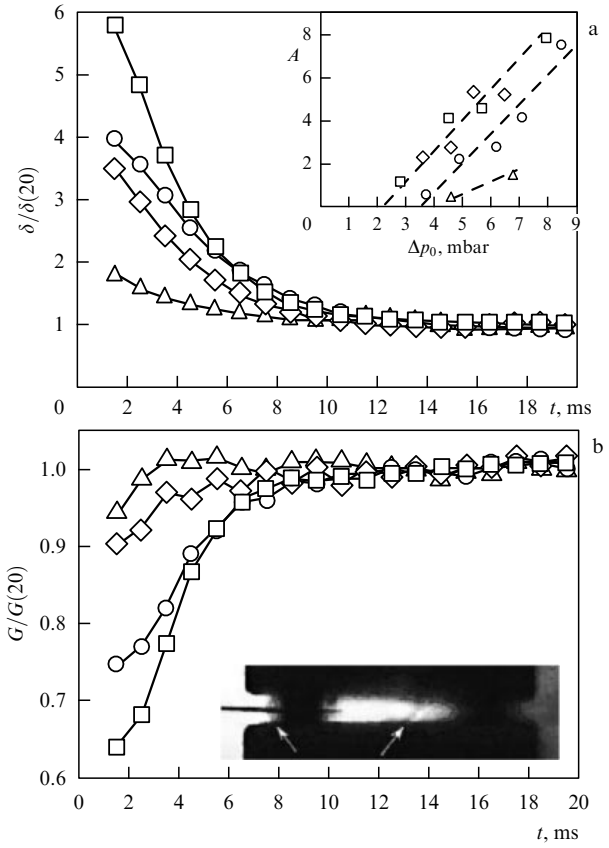

Figure 17. Relaxation of internal friction in a crystal grown in a burstlike mode at $T = 0.49$ K [49]. (a) Variations of the logarithmic decrement with respect to the stationary value after 20 ms. Starting supersaturations: 2.8 mbar (triangles), 4.5 mbar (diamonds), 5.7 mbar (circles), and 8 mbar (squares). The inset shows the dependence of parameter A obtained by approximation of the dependences with formula (7) on the starting supersaturation at four temperatures: squares — 0.49 K, diamonds — 0.59 K, circles — 0.65 K, and triangles — 0.69 K. (b) Respective change in normalized averaged shear modulus. Inset displays photograph of a helium crystal grown in the gap between the base and the quartz resonator. Arrows indicate crystal boundaries.

The addition to the decrement increases with increasing initial supersaturation pressure and tends to zero on approaching the boundary that separates normal and anomalous growth regions (see the inset to Fig. 17). Characteristic relaxation time $\tau \approx 3$ ms remains unaltered in a temperature range of 0.5–0.7 K. A monotonic increase in the elastic modulus tracked decrement variations. In the context of the relaxation model, an increase in the modulus suggests extension of the relaxation time of the dissipative process responsible for damping.

Unfortunately, these results elude unambiguous interpretation. Excess damping can be both a consequence of the altered internal state of the crystal, influencing dissipative processes during dislocation segment oscillations, and an obvious result of the annealing of nonequilibrium dislocation grid produced by fast growth, as in preceding experiments [36].

4.8 Attempt to create a stationary anomalous state

The short lifetime of the anomalous state imposes limitations on the choice of methods for its investigation. An attempt to prepare a quasistationary anomalous state was undertaken in Ref. [50]. The necessary supersaturation was produced hydrodynamically. To this end, a crystal was placed on a Π-shaped superconducting loop in a magnetic field (Fig. 18). Alternating current carried by the crystal induced its vibrations and thereby generated excess pressure on its parts facing the oncoming flow. Oscillators used in the present experiment operated at a frequency of ≈ 200 and ≈ 800 Hz, and supersaturation was achieved within around 1 ms. A sharp change in the kinetics of this segment or the entire crystal surface (as could be expected from previous experiments) altered both the eigenfrequency registered and the Q-factor of the system. Because fast facet growth kinetics persisted within ≈ 3 ms after transition to the anomalous phase (see Fig. 12), it was expected that the anomalous phase should exist and become stationary during the oscillation half-period till the next supersaturation maximum. This did not happen, however, because of an instability origination that resulted in the crystal 'sliding down' from the oscillator crossbar after the amplitude rate of ≈ 3 cm s^{-1} was reached, even when the crossbar pierced the crystal (Fig. 18a).

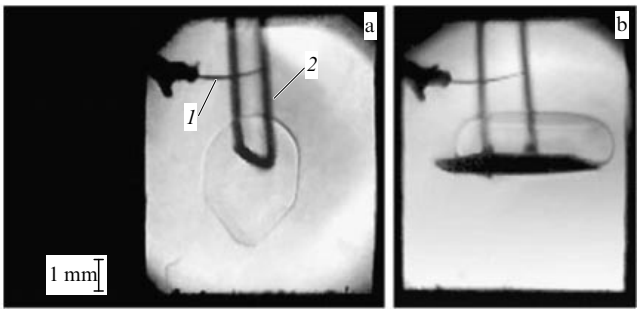

Figure 18. Vibrations of a helium crystal in a superfluid liquid [50]. The crystal formed on needle *1* and then remelted so as to be either pierced by the Π-shaped superconducting loop *2* (a) or located on a platform glued to the loop (b).

5. Main qualitative features of the effects and attempts to explain them

Investigations into the growth kinetics of helium crystal facets at large departures from equilibrium have revealed two qualitatively new effects that drop out from the well-known and experimentally verified picture of layer-by-layer growth of the crystal surface, including that of helium crystals at small departures from equilibrium. These are the superslow growth of perfect *c*-facets free from growth defects and the abnormally fast growth of facets having or not having growth sources. It is still difficult to judge whether they are related by a common mechanism or have different physical natures. They are similar to each other in terms of two experimental facts, viz. the enhancement of growth rate with decreasing temperature and the comparable effect of introduction of a small isotopic impurity.

5.1 Superslow facet growth

The main qualitative features of superslow facet growth are as follows:

• the growth rate is constant at temperatures up to ≈ 10 mK but decreases by an order of magnitude as the temperature approaches ≈ 100 mK; in other words, a rise in temperature slows down crystal growth;

• the introduction of an impurity of ^{3}He at a concentration of 100 ppm or higher into the fluid decreases the growth rate roughly threefold regardless of temperature.

Thus far, the sole theoretical explanation of superslow growth of helium crystals in the absence of impurities is that proposed by Andreev and Melnikovsky [51]. In accordance with their model, vacancies are generated at the atomically rough crystal–substrate interface. Then, the vacancies diffuse toward the crystal–liquid interface at which they annihilate and thereby cause facets to grow. The growth rate V is proportional to the applied supersaturation δp, while facet mobility $\mu_f = V/\delta p$ depends on temperature:

$$\mu_f \sim \left[\frac{\text{const}}{\sqrt{T}} \exp\left(\frac{\varepsilon_0}{T}\right) + \text{const}\sqrt{T} \exp\left(\frac{-\Delta_U}{T}\right)\right]^{-1}, \quad (8)$$

where ε_0 is the bottom of the vacancion zone, and Δ_U is the transposition parameter. The authors of Ref. [51] report no numerical estimates. They considered three possibilities for experimental verification of the model based on observing the dependence of the facet growth rate on the thickness, the presence of maximum growth rate for the temperature dependence according to formula (8), and the displacement of an object frozen in the crystal in the course of facet growth.

5.2 Qualitative features of burstlike growth

The assumption that the observed acceleration of perfect *c*-facet growth in the millikelvin region in crystals grown on a needle with a dislocation concentration of $\sim 10^5$ cm^{-2} is based on the following general qualitative experimental facts:

• a sharp transition from slow to fast *c*-facet growth kinetics;

• critical supersaturations at which the anomalous growth begins are similar in magnitude and temperature dependence;

• time of formation of the anomalous state decreases with increasing supersaturation;

• introduction of an additional dissipation channel (an impurity) into the fluid affects both critical supersaturation and time of formation of the anomalous state in a similar manner.

A comprehensive analysis of the above facts makes it possible to exclude from consideration quite a few potential sources of the effect. The observation of burstlike growth on defect-free facets rules out models relating the mechanism to dislocation dynamics, e.g., 'pumping' the dislocation grid energy by a spiral growth step or producing a vortex ring by the Frank–Read source.

Integration of qualitative features revealed in both experiments yields the following list of requirements for the future theory of the phenomenon in question.

(1) Transition is initiated by the excess pressure (supersaturation).

(2) Macroscopic time is needed for growth acceleration to start (under certain conditions, a few dozen seconds).

(3) Crystal structure (the presence or absence of defects) has no crucial effect on the preparation of the burstlike growth state.

(4) The most conspicuous feature of the phenomenon is simultaneous acceleration by a few orders of magnitude of the growth rate of facets regardless of their crystallographic orientation with respect to the rates sustained by the known mechanisms of layer-by-layer growth due to growth defects (spiral growth, Frank–Read sources).

(5) Both critical supersaturation giving rise to a fast growth state and the time it takes to be prepared depend on dissipation in the fluid: the two parameters increase upon a rise in temperature and the introduction of a diffusion channel of dissipation due to ^{3}He impurities.

(6) Once growth is completed and phase pressure equilibrium established, the facet kinetics continuously return to the normal (slow) ones in a macroscopic time up to 1 s; growth defects are not generated in the process.

5.3 Mechanisms of accelerated growth of an atomically smooth surface

Let us consider the known processes underlying facet growth acceleration with respect to the effect of interest. One mechanism markedly accelerating facet growth with increasing supersaturation, as postulated in the layer-by-layer growth model, is due to transition from dislocation-driven growth to active two-dimensional nucleation with exponential dependence of the growth rate $V \sim \exp(-\text{const}/\delta\mu^n)$, where $n = 1-2$ [1, 12, 13]. It is an attractive possibility, because cumulative distributions of the probability of fast growth origination (Fig. 10a) are well approximated by this dependence. The qualitative features of the growth due to

two-dimensional nucleation are consistent with those covered by points 1–3 of the above list (see Section 5.2). However, this mechanism cannot explain the remaining peculiarities of the effect. For example, the temperature dependence of critical supersaturation in the phase diagram (see Fig. 11) is opposite to that expected for the nucleation mechanism. On the other hand, supersaturation necessary for the formation of a three-dimensional nucleus in metastable superfluid helium increases to a constant value as temperature drops and subbarrier nucleation begins to prevail [14, 52–54]. The height of the barrier to be overcome by the nuclei is given by the linear step energy β on the surface, which is different for facets of different orientations. The value of β depends on how close the temperature is to the roughening transition temperature for a given facet [55]. These factors would be responsible for the origination of *a*-, *c*-, and *s*-facet growth due to nucleation at different supersaturations, in conflict with experimental data.

The second mechanism accelerating facet growth rate is associated with the breakup of the roughening phase transition. Nozieres and Gallet [56] showed, in the framework of the renormalization group formalism, that excess pressure causes the roughening transition to spread, and the facet below the transition point retains mobility in the absence of growth defects. The effect passes a maximum at temperatures close to T_R and weakens when the temperature deviates from T_R [57]. Spreading of the roughening transition for each facet family will occur at different temperatures, which prevents simultaneous growth acceleration of all facets. The temperature dependence of facet growth predicted in Ref. [53] is the opposite to that associated with the effect of burstlike growth.

Gov [58] mainly considered the formation of a critical nucleus in a metastable fluid with the emergence of vortices but tried to employ the same approach in one of the sections of an article to explain the burstlike growth. This model essentially makes use of two circumstances: the closeness to roughening transition described by the Kosterlitz–Thouless formalism, and the presence of growth sources. The author of Ref. [58] notes that his model does not account for the time lag between crystal origination and the onset of the rapid growth.

The authors of Refs [59, 60] proposed a model of growth acceleration by kinematic multiplication of steps on crystal facets. In this model, the number of steps increases due to both reciprocal collisions and spontaneous barrierless multiplication of an individual step when the threshold supersaturation is exceeded. As a result, a rise in step concentration increases the number of sites for the barrierless attachment of fluid atoms to the surface and speeds up facet growth by the mechanism described in the Introduction. Unfortunately, this approach, too, fails to account for all qualitative features of burstlike growth as emphasized by the authors of Refs [59, 60] themselves; moreover, its value is not confirmed by numerical calculations. At temperatures above 0.15 K, dissipation during step movements prevents their acceleration to velocities needed to initiate the process, and neither kinematic multiplication of the steps nor acceleration of facet growth occur at supersaturations observed in experiments.

5.4 The surface or the bulk?

Attempts to explain the effect of burstlike crystal growth by changes in the kinetics of the surface alone encounter serious difficulties. Because the growth of *a*-, *c*-, and *s*-facets having different parameters (interplanar spacing, roughening transition temperature, surface energy) occurs simultaneously and proportionally, the assumption of a purely surface mechanism behind kinetic changes must explain its insensitivity to these parameters.

The simultaneous transition of all facets to the fast growth state is easy to explain if the crystal bulk state changes. The new state is likely to have different surface characteristics that may cause a reverse transition of facets from the atomically smooth to the atomically rough state and thereby provide sustaining the fast growth rate. The faceting observed at the fast growth stage can be attributed to its kinetic nature, similar to that on helium crystals at temperatures above the first roughening transition point [17]. The assumption of the volumetric character of crystal transformation is confirmed indirectly by observing internal friction relaxation (see Section 4.7.2). However, the hypothesis of the volumetric character of the burstlike growth effect must explain how additional dissipation caused by the introduction of a minor ^{3}He impurity into the fluid can strongly influence the preparation of the burstlike growth state. That in the millikelvin region the impurity remains specifically in the fluid follows from the phase diagram of a weak ^{3}He$-^4$He solution.

Thus, only general considerations are pertinent as regards the new mechanism of fast crystal growth based on the main qualitative features of the phenomenon of interest. The substantial delay of the onset of burstlike growth is due either to the accumulation of a certain critical factor or to the fluctuational preparation of this state. The former conjecture better explains the gradual return to slow kinetics in equilibrium, i.e., decay of the accumulated factor. Unfortunately, these general considerations clarify neither the nature nor the source of this factor.

For the candidates destroying faceting and returning a crystal surface to an atomically rough state, A F Andreev postulated peculiar dislocation defects — that is, semirings located near the crystal surface. He showed that taking account of thermal fluctuations leads to the atomically rough state of the crystal surface at any temperature [61]. If the effect is of a volumetric character, e.g., the accumulation of vacancies, then a decrease in mean density results in the reduction of energies of point defect generation, i.e., vacancies proper. Such energy rearrangement after a critical concentration is reached will probably lead to the phase transition to a new state, possibly even to a supersolid state, which has been a subject of extensive discussion during the past decade in light of the discovery of the nonclassical behavior of the solid-helium moment of inertia by Kim and Chan [37, 38]. However, numerical simulation of helium crystals by the quantum Monte Carlo method reported by Pollet et al. [62] showed that the energy of vacancy formation falls to zero when the molar volume increases by $\sim 13\%$. Such a striking alteration of crystal density was not observed in experiment.

5.5 Prospects for further research

The list of experimental techniques for the study of the phenomenon of interest is rather short. Clearly, further research should be continued by extending the same methods to the ultralow temperature region if new qualitative data are to be obtained. For freely growing crystals, this implies calorimetric measurements of the state formation process (see Section 4.7.1), bearing in mind that a drop in temperature decreases the thermal response of adiabatic pressure oscilla-

tion in the container in proportion to T^3, while an increase in the kinetic facet growth coefficient lowers dissipative heating. When the fast growth state is prepared due to bulk transition, it can be hoped that the temperature of this transition will be possible to measure upon suppression of auxiliary thermal contributions.

A much longer time for preparing a helium crystal with the perfect *c*-facet for the transition to the burstlike growth state would allow measuring heat conductivity during slow growth and its dependence on the vacancy flow, provided the mechanism postulated in Ref. [51] operates (see Section 5.1). The proposals of the authors of this work have not yet been implemented. The kinetics of the dislocation-free *c*-facet of the crystal at the fast growth stage (see Section 4.2.1) have been remained unexplored, the inertia of the pressure gauge in experiments [7] having been too high. A comparison of the fast growth kinetics of defective and defect-free facets in the common temperature range from 180 to 250 mK could provide additional arguments in favor of the identical or, conversely, the different natures of these phenomena.

The internal structure of a crystal in an anomalous state awaits investigation. Results of direct measurements of lattice parameters and the Debye–Waller factor, if different from the values for equilibrium crystals, would be conclusive evidence of bulk transition. Such measurements are possible with the aid of a short X-ray pulse synchronized with a fast growth stage. This method is most simple to realize at ^{3}He-refrigerator temperatures using synchrotron radiation sources with the necessary intensities for X-ray sources.

6. Conclusion

The present review disregarded other phenomena, e.g., instability of the crystal growth form, since they are consequences rather than causes of fast surface growth [63–65]. The primary objective of the review was to systematize and comprehensively expound experimental facts concerning the preparation of an anomalous state with a high facet growth rate. The phenomenon of an abrupt change in the growth kinetics of helium crystal facets remains unexplained, notwithstanding the 20-year history of its investigation. A physical mechanism needs to be found that underlies simultaneous acceleration of the growth of all facets regardless of their orientation. A specific feature of such a mechanism is that it must support the long-lasting action of supersaturation, from a few milliseconds to several dozen seconds, to enable preparation of the fast growth state. The fast facet growth kinetics once developed under high supersaturation persist long after completion of crystal growth and reaching phase equilibrium pressure; thereafter, it gradually becomes slower under the influence of growth defects in crystals grown on a needle or superslow on perfect facets. The available theoretical publications deal with selected aspects of the effect but cannot describe all of them taken together. Even such a seemingly obvious question as whether it is a change in the bulk properties of a crystal as opposed to the surface ones that lies behind the effect of interest has no definite answer.

A qualitatively new approach comes under the scrutiny of research.

Acknowledgments

The author is grateful to Yu M Kagan, L A Maksimov, S N Burmistrov, and L B Dubovskii of the National Research Centre 'Kurchatov Institute' for many fruitful discussions during the entire period of this work, and to V S Kruglov and V A Sharykin for the support of the experimental part. A Ya Parshin, unfortunately deceased, formerly affiliated with the Kapitza Institute for Physical Problems, Russian Academy of Sciences, made invaluable contributions to the discussion of all aspects of the effect. Thanks are due to A F Andreev for the opportunity to continue experiments at the Kapitza IPP RAS and to V V Zav'yalov for assistance without which this work could hardly have been done at all. The work was supported for many years by the Russian Foundation for Basic Research (grants 93-02-2587a, 96-02-1811a, 99-02-17289a, 02-02-16772a, and 05-02-16806a).

References

1. Chernov A A et al. *Modern Crystallography* Vol. 3 *Crystal Growth* (Berlin: Springer-Verlag, 1984); Translated from Russian: *Sovremennaya Kristallografiya* Vol. 3 *Obrazovanie Kristallov* (Ed. B K Vainshtein) (Moscow: Nauka, 1980)
2. Andreev A F, Parshin A Ya *Sov. Phys. JETP* **48** 763 (1978); *Zh. Eksp. Teor. Fiz.* **75** 1511 (1978)
3. Balibar S, Alles H, Parshin A Ya *Rev. Mod. Phys.* **77** 317 (2005)
4. Straty G C, Adams E D *Phys. Rev. Lett.* **17** 290 (1966)
5. Tsymbalenko V L *Instrum. Exp. Tech.* **40** 585 (1997); *Prib. Tekh. Eksp.* (4) 161 (1997)
6. Tsymbalenko V L *Cryogenics* **36** 65 (1996)
7. Hakonen P J et al. *J. Low Temp. Phys.* **101** 41 (1995)
8. Ruutu J P et al. *J. Low Temp. Phys.* **112** 117 (1998)
9. Keshishev K O, Parshin A Ya, Babkin A V *JETP Lett.* **30** 56 (1979); *Pis'ma Zh. Eksp. Teor. Fiz.* **30** 63 (1979)
10. Wolf P E et al. *J. Physique* **46** 1987 (1985)
11. Tsymbalenko V L *Low Temp. Phys.* **21** 120 (1995); *Fiz. Nizk. Temp.* **21** 162 (1995)
12. Andreev A F, in *Quantum Theory of Solids* (Ed. I M Lifshits) (Moscow: Mir Publ., 1982) p. 11
13. Uwaha M *J. Low Temp. Phys.* **52** 15 (1983)
14. Tsymbalenko V L *J. Low Temp. Phys.* **88** 55 (1992)
15. Landau L D, Lifshitz E M *Fluid Mechanics* (Oxford: Pergamon Press, 1987); Translated from Russian: *Gidrodinamika* (Moscow: Nauka, 1986)
16. Tsymbalenko V L *JETP* **92** 1024 (2001); *Zh. Eksp. Teor. Fiz.* **119** 1182 (2001)
17. Tsymbalenko V L *J. Low Temp. Phys.* **121** 53 (2000)
18. Tsymbalenko V L *JETP* **99** 1214 (2004); *Zh. Eksp. Teor. Fiz.* **126** 1391 (2004)
19. Castaing B, Balibar S, Laroche C *J. Physique* **41** 897 (1980)
20. Bodensohn J, Nicolai K, Leiderer P *Z. Phys. B* **64** 55 (1986)
21. Ruutu J P et al. *Phys. Rev. Lett.* **76** 4187 (1996)
22. Tsymbalenko V L *Phys. Lett. A* **211** 177 (1996)
23. Tsymbalenko V L *Phys. Lett. A* **248** 267 (1998)
24. Tsymbalenko V L *Phys. Lett. A* **257** 209 (1999)
25. Tsymbalenko V L *J. Low Temp. Phys.* **138** 795 (2005)
26. Tsymbalenko V L *JETP Lett.* **77** 243 (2003); *Pis'ma Zh. Eksp. Teor. Fiz.* **77** 288 (2003)
27. Tsymbalenko V L *Phys. Lett. A* **274** 223 (2000)
28. Esel'son B N et al. *Rastvory Kvantovykh Zhidkostei* He^3–He^4 (Solutions of He^3–He^4 Quantum Liquids) (Moscow: Nauka, 1973)
29. Burmistrov S N, Dubovskii L B *Europhys. Lett.* **24** 749 (1993)
30. Castaing B, Greenberg A S, Papoular M *J. Low Temp. Phys.* **47** 191 (1982)
31. Treiner J *J. Low Temp. Phys.* **92** 1 (1993)
32. Tsymbalenko V L *JETP* **81** 373 (1995); *Zh. Eksp. Teor. Fiz.* **108** 686 (1995)
33. Tsymbalenko V L *JETP Lett.* **78** 493 (2003); *Pis'ma Zh. Eksp. Teor. Fiz.* **78** 965 (2003)
34. Tsymbalenko V L *Sov. Phys. JETP* **47** 787 (1978); *Zh. Eksp. Teor. Fiz.* **74** 1507 (1978)
35. Paalanen M A, Bishop D J, Dail H W *Phys. Rev. Lett.* **46** 664 (1981)
36. Tsymbalenko V L *Sov. Phys. JETP* **60** 537 (1984); *Zh. Eksp. Teor. Fiz.* **87** 943 (1984)

37. Kim E, Chan M H W *Nature* **427** 225 (2004)
38. Kim E, Chan M H W *Science* **305** 1941 (2004)
39. Day J, Beamish J *Nature* **450** 853 (2007)
40. Day J, Syshchenko O, Beamish J *Phys. Rev. B* **79** 214524 (2009)
41. Syshchenko O, Day J, Beamish J *Phys. Rev. Lett.* **104** 195301 (2010)
42. Haziot A et al. *Phys. Rev. B* **88** 014106 (2013)
43. Haziot A et al. *Phys. Rev. Lett.* **110** 035301 (2013)
44. Fefferman A D et al. *Phys. Rev. B* **89** 014105 (2014)
45. Mason W P (Ed.) *Physical Acoustics* Vol. 4 Pt. A *Applications to Quantum and Solid State Physics* (Amsterdam: Elsevier, 1966); Translated into Russian: *Fizicheskaya Akustika* (Ed. W Mason) Vol. 4 Pt. A *Primenenie Fizicheskoi Akustiki v Kvantovoi Fizike i Fizike Tverdogo Tela* (Moscow: Mir, 1969)
46. Tsymbalenko V L *Phys. Lett. A* **353** 87 (2006)
47. Tsymbalenko V L *JETP* **103** 869 (2006); *Zh. Eksp. Teor. Fiz.* **130** 1006 (2006)
48. Tsymbalenko V L *Phys. Lett. A* **378** 2325 (2014)
49. Tsymbalenko V L *JETP* **119** 700 (2014); *Zh. Eksp. Teor. Fiz.* **146** 794 (2014)
50. Tsymbalenko V L *J. Low Temp. Phys.* **171** 21 (2013)
51. Andreev A F, Melnikovsky L A *JETP* **93** 1261 (2001); *Zh. Eksp. Teor. Fiz.* **120** 1457 (2001)
52. Lifshitz I M, Kagan Yu *Sov. Phys. JETP* **35** 206 (1972); *Zh. Eksp. Teor. Fiz.* **62** 385 (1972)
53. Ruutu J P et al. *Phys. Rev. Lett.* **77** 2514 (1996)
54. Sasaki Y, Mizusaki T *J. Low Temp. Phys.* **110** 491 (1998)
55. Keshishev K O, Marchenko V I, Shemyatikhin D B *JETP* **116** 587 (2013); *Zh. Eksp. Teor. Fiz.* **143** 674 (2013)
56. Nozieres P, Gallet F *J. Physique* **48** 353 (1987)
57. Wolf P E et al. *J. Physique* **46** 1987 (1985)
58. Gov N *J. Low Temp. Phys.* **129** 25 (2002)
59. Parshin A Ya, Tsymbalenko V L *JETP Lett.* **77** 321 (2003); *Pis'ma Zh. Eksp. Teor. Fiz.* **77** 372 (2003)
60. Parshin A Ya, Tsymbalenko V L *JETP* **103** 278 (2006); *Zh. Eksp. Teor. Fiz.* **130** 319 (2006)
61. Andreev A F *JETP Lett.* **52** 619 (1990); *Pis'ma Zh. Eksp. Teor. Fiz.* **52** 1204 (1990)
62. Pollet L et al. *Phys. Rev. Lett.* **101** 097202 (2008)
63. Burmistrov S N, Dubovskii L B, Tsymbalenko V L *Phys. Rev. E* **79** 051606 (2009)
64. Dubovskii L B, Burmistrov S N, Tsymbalenko V L *J. Low Temp. Phys.* **162** 391 (2011)
65. Dubovskii L B, Burmistrov S N, Tsymbalenko V L *J. Low Temp. Phys.* **162** 383 (2011)